Ocean Engineering 313 (2024) 119380

Contents lists available at ScienceDirect

Ocean Engineering

journal homepage: www.elsevier.com/locate/oceaneng

Research paper

Assessment of the effectiveness of ship machinery noise reduction measures using a test platform in a water basin

Marc-André Guy [a,b,*], Kamal Kesour [b], Mathis Vulliez [a,b], Stéphane Gagnon [b], Julien St-Jacques [b], Raphael Tremblay [b], Jean-Christophe Gauthier Marquis [b], Olivier Robin [a,b]

[a] Centre de Recherche Acoustique - Signal - Humain, Université de Sherbrooke, 2500 Boulevard de l'Université, J1K 2R1, Sherbrooke, Québec, Canada
[b] Innovation maritime, 53 rue Saint-Germain Ouest, G5L 4B4, Rimouski, Québec, Canada

ARTICLE INFO

Keywords:
Underwater radiated noise
Commercial shipping
Machinery noise
Noise control
Mitigation technologies
Test platform
Water basin

ABSTRACT

Underwater radiated noise (URN) from commercial shipping is partly responsible for increased ocean ambient noise levels in the last decades. To preserve marine wildlife, there is a need to reduce it. Machinery noise is the dominant URN source at lower speeds. Mitigation technologies exist to reduce it, but a lack of quantitative data regarding their effectiveness results in limited practical ship applications since the cost-to-benefit ratio is imprecise. A small ship-like structure (test platform) representative of a ship section is designed and constructed to conduct measurements in a controlled environment and at a lower cost than actual on-ship testing. The platform is deployed in a water basin whose acoustic response is first characterized by reverberation measurements. Vibroacoustic sources simulate structure-borne and airborne noise, while hydrophones and sensors measure the response in the water basin and of the platform. Measurements with and without standard mitigation technologies installed in the platform are conducted to quantify the insertion loss. Up to 37 and 20 dB URN reductions are obtained with elastic mounts and mineral wool, respectively. The results obtained with the platform and the developed methodology can support and guide the implementation of mitigation measures in current and future ship constructions.

1. Introduction

Overall ambient noise levels in the open ocean have increased at approximately 3 dB per decade since 1950 (Andrew et al., 2002; Frisk, 2012). The low-frequency range (i.e., below 500 Hz) is mainly affected by this increase (Andrew et al., 2010; McKenna et al., 2012). The growth in these noise levels is correlated to commercial shipping activity and global economic growth (Frisk, 2012; Hildebrand, 2009; Mcdonald et al., 2008; Tournadre, 2014). This correlation was well illustrated during the COVID-19 pandemic: the overall reduction of human activities, including maritime traffic, led to reduced noise levels in urban and natural areas (Zambon et al., 2021; Terry et al., 2021). Underwater noise levels at low frequencies were persistently and significantly lower during this pandemic (Robinson et al., 2023; Ryan et al., 2021).

Underwater noise affects marine wildlife's habitat quality (Putland et al., 2017) and impacts its behavior because acoustic signals are essential for feeding, communicating, reproducing, and detecting predators or prey. Underwater noise also significantly stresses marine mammals (Williams et al., 2015; Erbe et al., 2019; Gervaise et al., 2012; Murchy et al., 2019), and even marine invertebrates (Gigot et al., 2024). The already important contribution of commercial shipping to ambient ocean noise levels is expected to rise, with the projected percentage increase in sound exposure levels in 2030 relative to 2015 being 53% for container ships and reaching 192% for bulk carriers (Kaplan and Solomon, 2016). The effects of climate change should bring cumulative effects to this situation by facilitating sound propagation in the oceans (Possenti et al., 2023, 2024). The need to identify and implement concrete solutions for reducing underwater radiated noise (URN) from commercial navigation is now a priority, as highlighted by the International Maritime Organization (IMO) recent 2023 guidelines (International Maritime Organization, 2023).

On large commercial ships such as oil tankers, container ships, or bulk carriers, underwater noise sources are generally divided into three distinct categories: (1) propeller-induced noise, including cavitation, (2) flow noise, mainly along the hull, and (3) machinery noise (Abrahamsen, 2012; Audoly et al., 2015; Kendrick and Terweij, 2019; Fischer, 2024). The first two sources usually dominate at high speed, while machinery noise dominates at low speed (ITTC, 2017;

* Corresponding author at: Centre de Recherche Acoustique - Signal - Humain, Université de Sherbrooke, 2500 Boulevard de l'Université, J1K 2R1, Sherbrooke, Québec, Canada.
E-mail address: marc-andre.guy@usherbrooke.ca (M.-A. Guy).

https://doi.org/10.1016/j.oceaneng.2024.119380
Received 8 August 2024; Received in revised form 16 September 2024; Accepted 25 September 2024
Available online 3 October 2024

Fischer, 2024). Machinery noise can be the dominant source for smaller ships, regardless of speed (Smith et al., 2024; Armelloni et al., 2022). To reduce underwater noise, reducing speed or optimizing the propeller are effective solutions (Smith and Rigby, 2022). However, propeller-based solutions are rarely considered given their high cost, and speed reduction implies a loss of competitiveness through a longer transport time. Even if these actions were adopted, machinery noise would remain an open issue. It is then important to find effective solutions to reduce machinery noise, as it dominates at low speeds, especially in ports, slowdown zones, and near protected areas.

Solutions exist to limit the contribution of machinery noise to URN, but the related research often focuses on a reduced number of solutions (Arveson and Vendittis, 2000; Audoly et al., 2017; Dylejko et al., 2016). In addition, the sizing rules that could be used at a design phase need to be better documented as well as the effectiveness of solutions to reduce URN (Smith and Rigby, 2022). Since their implementation on an existing ship or under construction is costly, shipowners need incentives and quantified performance guarantees before incorporating these technologies (Fischer, 2024). There is, therefore, a need to better document the overall performance of standard noise reduction measures in terms of levels and implementation to apply the 2023 IMO guidelines (International Maritime Organization, 2023). However, modifications or tests to an existing vessel are often complex and expensive. In practice, to quantify the actual performance of a noise reduction solution for a particular machine, noise coming from it must be isolated by turning off the other machines. This situation is challenging to achieve since a ship generally cannot operate with the machinery turned off. In addition, isolating underwater noise from a single vessel is an additional challenge since the noise of other vessels nearby may disrupt the measurements, as does ambient background noise. In short, operational constraints greatly complicate evaluating the effectiveness of noise and vibration control measures while such tests are already very costly (Cochard et al., 2000).

Testing can be conducted on a smaller scale and in a controlled environment to simplify and reduce the cost of measurements. Laboratory test basins are an alternative to open-water facilities for calibrating underwater sound sources and transducers (Çorakçıet al., 2024; Cochard et al., 2000), but can also be used for structure-related tests. Donaldson (1968) used a floating steel panel in a water basin to study the effect of applying external coatings and damping treatment on radiated noise power. The MARIN team (Maritime Research Institute Netherlands) from the EU Horizon 2020 project SATURN (Developing Solutions to Underwater Radiated Noise) developed a scaled midship model based on a tanker hull geometry. The model evaluated insertion loss from an air injection system for reducing URN (Lloyd et al., 2023, 2024). Keizer et al. (2022) used a ship-like structure in an anechoic water basin to validate the accuracy of a numerical model in predicting underwater noise. Lee et al. (2023) designed floating plate structures in a reverberant water basin to measure underwater acoustic radiation efficiency. This radiation efficiency was then used in a numerical model to estimate the structure-borne URN transfer function of one of the structures (Lee et al., 2024). Fragasso et al. (2024) deployed a scaled mock-up model representing the machinery's foundation in a water basin, and transfer-path analysis was used to estimate underwater radiated noise.

Previous studies have used small-scale structures in a water basin, but none have investigated the actual URN reductions that standard mitigation technologies can obtain. To fill this technological gap, a test platform consisting of a small-scale structure representative of a section of a ship is designed and constructed in this study. The platform is deployed in a reverberant water basin and a rigorous test methodology is developed. The study's main contribution is to assess the platform's capacity to quantify the URN reduction provided by standard mitigation technologies currently used by ships and submarines. Conducting measurements in a water basin using a small ship-like structure offer the advantage of significantly reducing the costs associated with determining the acoustic effectiveness of URN mitigation technologies (labor and materials) compared to onboard full-scale measurements. In addition, several solutions can be independently evaluated on the same system and in a controlled environment.

The designed test platform, the acoustic response of the water basin and the developed methodology are first detailed in Section 2. Section 3 presents three noise reduction technologies commonly used on ships (elastic mounts, mineral wool and damping tiles) and their installation on the platform. The insertion loss evaluation procedure and uncertainty followed by the technologies' mitigation effectiveness are next presented in Section 4. Conclusions and future perspectives conclude the study in Section 5.

2. Test platform, its environment and followed methodology

2.1. Test platform

The test platform is a $3.5 \times 2.1 \times 1$ m^3 steel structure with a 6 mm thick plating (Fig. 1). A naval architect was consulted to design and dimension the platform to be comparable to a ship section in those elements such as girders, stiffeners, bulkheads, and a deckhead to capture the dynamic structural properties that could typically occur in a full-size vessel. The platform's hull thickness and materials were selected following the recommendations of the architect. No specific vessel class was considered in the design process, as the focus was to reach an "as usual as possible" design. The platform is, therefore, not a small-scale reproduction of a given reference ship: no scaling law was used to design it, given the task's complexity, and the study's goal is not to apply scaling laws to the obtained results. The maximal draught is 0.3 m: 41% of the exterior platform's surface is wetted. A mobile modular plate allows the attachment of vibroacoustic sources on the platform to simulate machinery. The plate can be fixed to 6 mm or 9 mm thick steel girders. Mechanical loads, i.e. different masses, can also be installed on the module to modify the draught of the platform and provide the right load for the tested elastic mounts. Work safety criteria were considered in the design to accommodate two people inside the platform for instrumentation, and the masses linked to the test systems. The upper part of the platform can be closed with 3 mm thick aluminum panels to confine noise inside the platform, just like an engine room, and prevent sound propagation in the basin. Overall, the design and manufacturing plans of the platform involved a multidisciplinary team, including the naval architect, mechanical engineers and technicians, and close consultation with a shipyard team.

An inertial shaker (Data Physics IV47-PA300E) is installed on the central plate to generate structure-borne noise. In contrast, airborne noise is created by an omnidirectional speaker (Bruel & Kjaer dodecahedral sound source type 4296). The operating frequency ranges of these two sources are 10 Hz to 2000 Hz and 50 Hz to 8000 Hz, respectively. Sensors positions are indicated in Fig. 2. A force sensor is installed directly under the vibration source to measure the force injected into the platform. Two microphones are positioned in the corners of the platform. Vibrations are measured using thirteen uniaxial accelerometers distributed on different platform areas and the plate where the vibration source is fixed. Eight triaxial accelerometers are positioned at the four corners of the plate, above and below the position where elastic mounts can be installed. A 16-channel analyzer (Oros 36, 24 bits) with a sampling frequency F_s of 25.6 kHz collects data from the force sensor, uniaxial accelerometers, and microphones and controls the two sources. Four 6-channel acquisition units (iDAQ, 24 bits, F_s = 25.6 kHz) developed by Innovation maritime are used to acquire data from the triaxial accelerometers. Fig. 3 shows sources and sensors installed inside the platform.

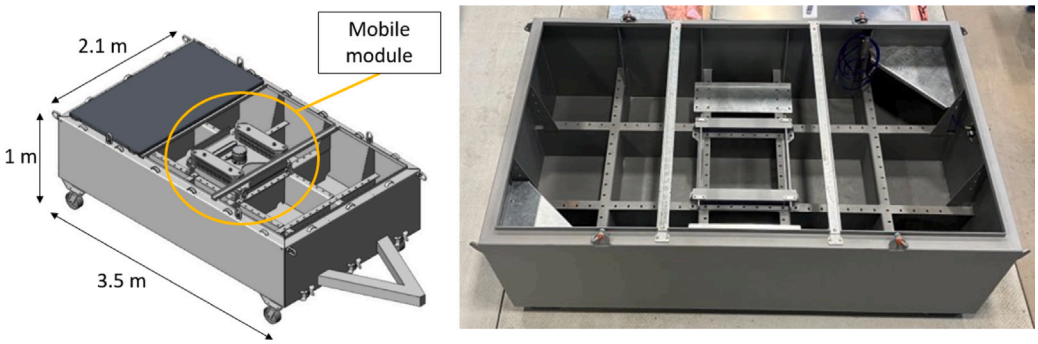

Fig. 1. (Left) Computer-aided design (CAD) file of the platform – (Right) Picture of the actual platform after mechanical realization.

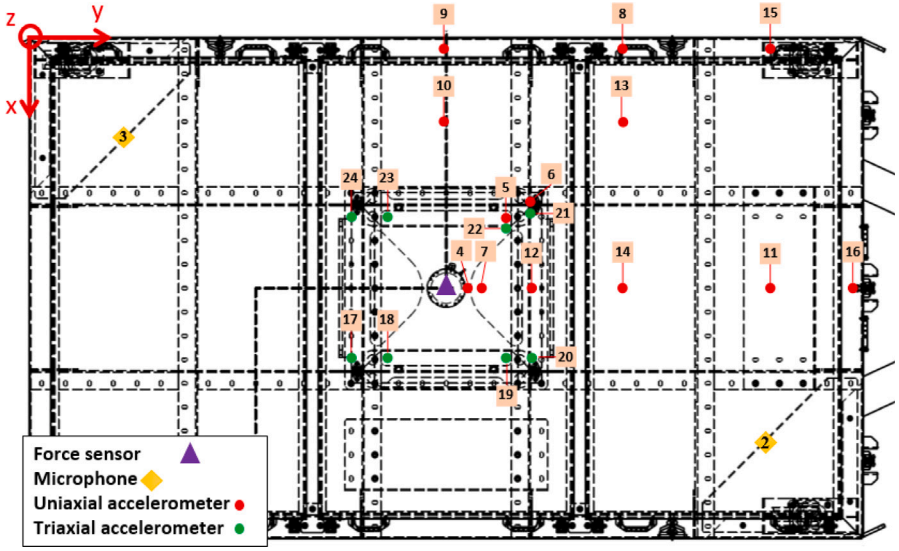

Fig. 2. Sensors positions.

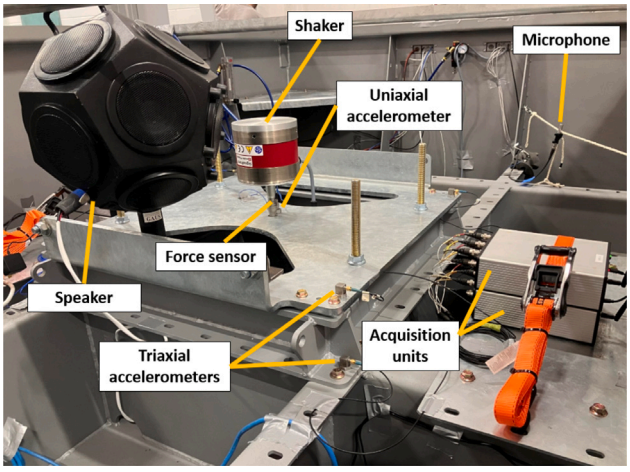

Fig. 3. Platform instrumentation setup.

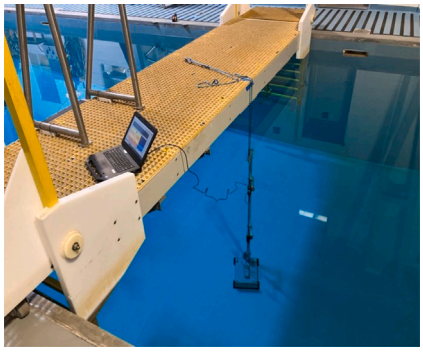

Fig. 4. Example of hydrophone array deployment in the basin using the dedicated frame.

2.2. Acoustic response of the water basin

2.2.1. Reverberation time

The water basin is a 15.0 × 5.1 × 3.4 m^3 diving basin located at Institut Maritime du Québec in Rimouski (QC, Canada). The basin walls are made of painted concrete and are thus highly reflective. Before installing the platform, it is fundamental to calibrate the test environment through reverberation time and direct field extension measurements as classically done in room acoustics (Cochard et al., 2000; Kuttruff, 2016). The water basin is first characterized by reverberation time measurements conducted following the interrupted source method (International Organization for Standardization, 2008). An underwater speaker (University Sound UW30) is fed by a pink noise signal from 10 Hz to 10 kHz. After the sound source is stopped, two hydrophones (Ocean Sonics, icListen RB9 HF, F_s = 32 kHz) measure the sound decay at two different depths with a dedicated and custom frame (see Fig. 4).

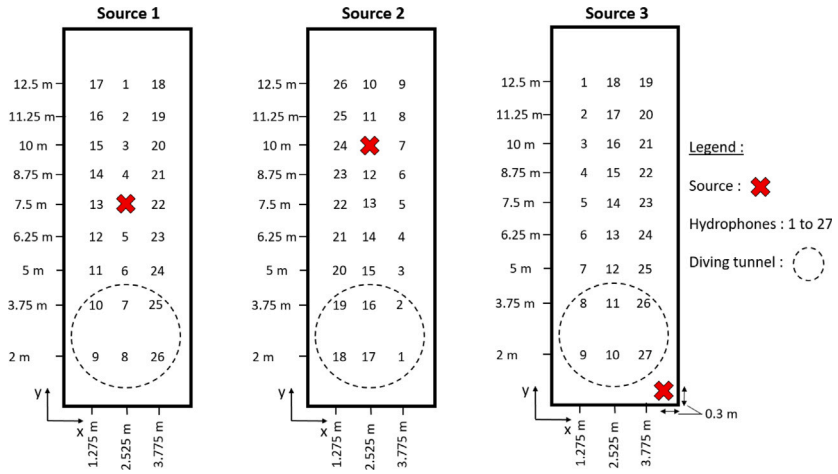

Fig. 5. Considered hydrophones' positions for each of the three positions considered for the acoustic source.

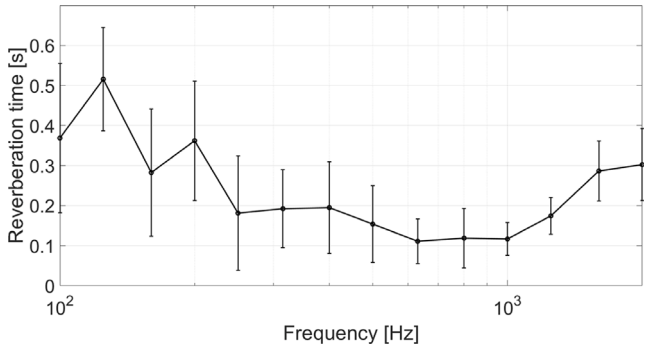

Fig. 6. Third octave reverberation times. Standard deviations are represented as vertical lines.

Three source positions in the basin are considered to obtain spatially averaged reverberation times. Hydrophones are positioned through the basin at 27 positions for each, and three decays are measured per position. The source and hydrophones' positions are summarized in Fig. 5.

For each decay, third octave reverberation times T_{60} are estimated using Schroeder's reverse integration technique (Schroeder, 1965). The results are averaged for both hydrophones at all tested positions to obtain a spatially averaged T_{60}. Fig. 6 shows the obtained reverberation times in third-octave bands, with vertical lines indicating the standard deviations.

The average reverberation time is between 0.1 s and 0.55 s for the different frequency bands, in agreement with values obtained by similar studies using reverberant basin (Cochard et al., 2000; Zhang et al., 2018). The frequency-averaged reverberation time is 0.24 s, lower than the value of 0.39 s obtained in Cochard et al. (2000), who conducted measurements in a more extensive water basin but on a different frequency domain (1 kHz to 20 kHz). Such difference is, however, consistent with Sabine's theory stating that the reverberation time is proportional to the volume of the space under study (255 m^3 in this case, and 900 m^3 in Cochard et al. (2000)). Standard deviations are generally more significant in low frequencies and are attributed to the lower signal-to-noise ratio (SNR) for this frequency range.

2.2.2. Critical frequency and critical radius

The critical frequency f_c (Schroeder's frequency), in Hz, and the critical radius R_c, in meters, are computed from the measured reverberation times using Eqs. (1) and (2):

$$f_c = \sqrt{\frac{c^3 T_{60}}{4V \ln(10)}}, \tag{1}$$

$$R_c = \sqrt{\frac{\ln(10^6) V}{4\pi c T_{60}}}, \tag{2}$$

where c is the sound speed in water (1500 m/s), V is the volume of the enclosure (255 m^3), and T_{60} is the 60-dB reverberation time in seconds (Schroeder, 1996).

The calculated critical frequency f_c is 620 Hz for the basin, whose order of magnitude is similar to other water basins (Cochard et al., 2000; Trinh et al., 2018). Critical frequency f_c corresponds to the frequency from which the sound field in the basin can be considered reverberant; the modal density above this frequency is sufficiently large such that the pressure level in the basin does not vary significantly in space. Below this frequency, sound pressure levels will highly depend on the spatial position of a hydrophone within the basin, given its modal behavior. The critical radius R_c is the distance from the source at which the direct sound level becomes equal to the one of reflected sound (Zhang et al., 2018; Trinh et al., 2018). The maximum value obtained through all bands is 1.25 m. Positioning the hydrophones at a larger distance than the critical radius from the source theoretically ensures that the reverberant field dominates the direct field. In summary, sound pressure levels should be independent of a hydrophone position when positioned at least 1.25 m from the source and for frequencies above the critical frequency of 620 Hz. When these conditions are unmet, the precise positioning of hydrophones becomes crucial. Repeatability in hydrophone positioning from one test to another must be ensured to evaluate the URN reduction of a given technology properly. This is guaranteed through a procedure and specially designed mechanical support as detailed in Section 2.3.

2.3. Testing methodology

A multi-parameter and iterative methodology is used to evaluate mitigation effects (Fig. 7). For each platform configuration, different loads (0 kg to 240 kg) are added to the plate supporting the shaker, and three other positions are possible for the sources on the platform (1 to 3, Fig. 8). An array of three hydrophones (1, 1.5, and 2 m from the bottom) is used (Fig. 9). For each configuration and load, the array is located at positions inside the basin (Fig. 8) based on the critical

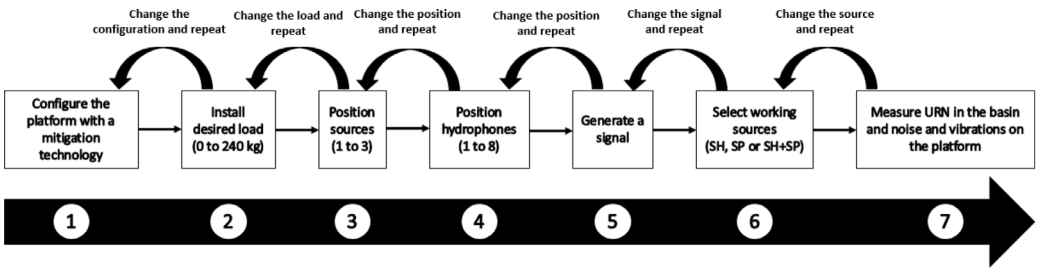

Fig. 7. Adopted iterative methodology.

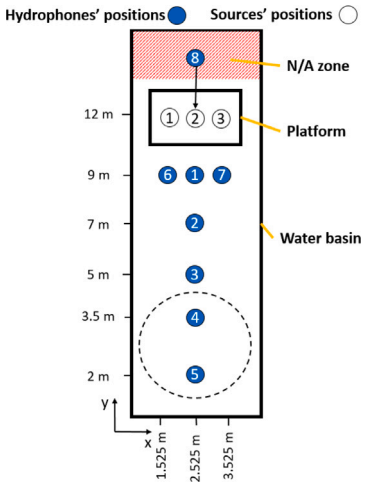

Fig. 8. Hydrophones and sources positions.

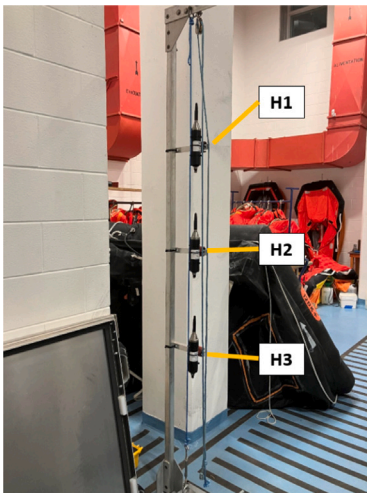

Fig. 9. Hydrophone array.

radius R_c. Repeatability in hydrophone positioning is ensured by using a precise coordinate system on the side of the basin. The sources successively generate tonal noise (at 60 Hz, 120 Hz, and 240 Hz), pink noise (10 Hz to 2000 Hz), and realistic signals at each hydrophone position. Realistic signals correspond to measurements recorded by a microphone and an accelerometer on a small ship with a 4-stroke diesel engine and converted to amplitude-normalized WAV files used to feed the speaker and the shaker, respectively. For each mitigation mean, individual shaker (SH) and speaker (SP) excitations are first considered and then combined (SH+SP) to isolate the effects of mitigation technologies on each vibroacoustic transmission path. Hydrophones measure URN in the basin for each excitation signal while force, noise, and vibration data are collected with the various sensors within the platform (Fig. 2). Sampling frequencies F_s are 32 kHz for hydrophones and 25.6 kHz for all sensors inside the platform. Along with the configurations with mitigation technologies installed, a reference case without any technologies is also tested to evaluate insertion loss (IL). All testing is conducted with the platform's top panels closed to prevent a direct airborne path between the platform and the basin and ensure that airborne noise is transmitted mostly through the platform plating. The platform's position within the basin is the same for all measurements: ropes are used to position it at set distances from the basin's walls. Since the platform is not in contact with any walls (except through ropes, whose vibration transmission is negligible), all structure-borne noise is transmitted through the platform plating.

3. Tested noise reduction solutions

3.1. Elastic mounts

3.1.1. Theoretical background

Elastic mounts are frequently used in the marine industry to reduce structure-borne noise contributions to URN by isolating vibrating machinery from the hull. A single-degree-of-freedom mass–spring model represents the mount-machine system. It is characterized by the mount's stiffness k (in N/m) and the machine's mass m (in kg). The system's natural frequency f_n (in Hz) is given by Eq. (3):

$$f_n = \frac{1}{2\pi}\sqrt{\frac{k}{m}} = \frac{1}{2\pi}\sqrt{\frac{g}{d}}, \tag{3}$$

where $g = 9.81$ m/s^2 is the gravitational acceleration and d (in m) is the mount's static deflection due to the machine's mass. The isolation effectiveness of the system corresponds to the transmissibility T, the ratio of the acceleration going into the system to the one flowing out of the system: the lower the transmissibility, the better the effectiveness. It is obtained with Eq. (4) according to István and Beranek (2005) and Fischer (2024):

$$T = \frac{A_{out}}{A_{in}} = \sqrt{\frac{1 + (2\zeta X)^2}{\left(1 - X^2\right)^2 + (2\zeta X)^2}}, \tag{4}$$

where A_{in} and A_{out} are the acceleration levels on the top and bottom surface of the mount, respectively, $X = f/f_n$ is the ratio of the excitation frequency f to the natural frequency f_n and $\zeta = C/C_c$ is the damping ratio. This is the ratio of the system's viscous damping coefficient C to its critical damping coefficient $C_c = 2\sqrt{km}$ (Fischer, 2024;

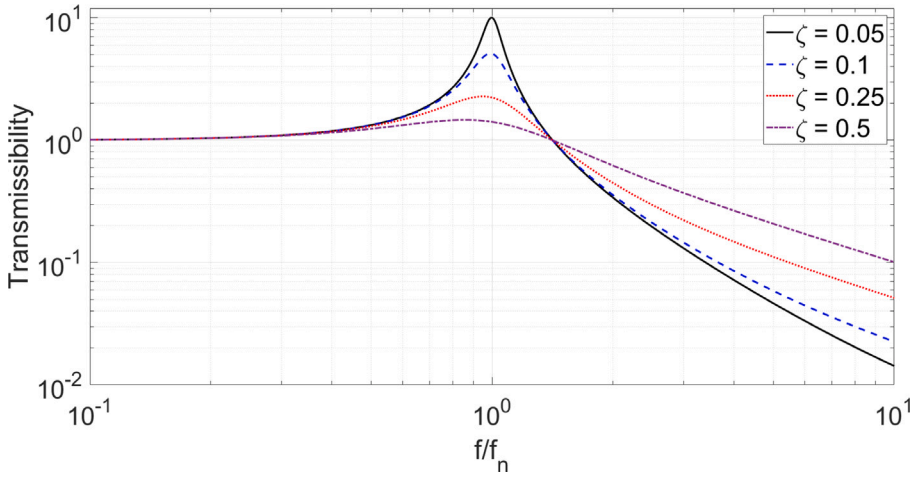

Fig. 10. Theoretical transmissibility for different damping ratio ζ.

István and Beranek, 2005). Fig. 10 presents theoretical transmissibility curves for different damping ratio values.

At very low frequencies ($f \ll f_n$), transmissibility is close to unity: the acceleration input equals the output, and the mounts practically have negligible effect. When the excitation frequency corresponds to the system's natural frequency ($f/f_n = 1$), transmissibility is maximal: this is the resonance zone in which the system can amplify input levels, depending on the value of the damping ratio. If no damping exists in the system ($\zeta = 0$), transmissibility approaches infinity at resonance. When $f \geq \sqrt{2} f_n$, mounts start to reduce vibration levels ($T < 1$): this is the zone to target while designing mounts to attenuate the vibrations transmitted to the hull. Most real systems have some level of dissipation or damping. Increasing the damping ratio ζ reduces transmissibility at resonance ($f = f_n$), but the trade-off is its increase above $f = \sqrt{2} f_n$. Mounts are usually designed so that the natural frequency is well below the lowest operating frequency of the machine to be isolated to avoid amplification around resonance and ensure effectiveness. Most vibration isolation systems in ships have a natural frequency between 5 Hz and 10 Hz (Fischer, 2024). Since mounts are designed to work in the $f \geq \sqrt{2} f_n$ zone, far from resonance, adding more damping leads to less vibration isolation. Typical damping ratios ζ for elastic mounts are usually around 0.05 to reach optimal isolation at higher frequencies (Fischer, 2024).

3.1.2. Selected mounts

Two models of elastic mounts (Mecanocaucho BRB-50, with two different hardness) are selected to evaluate the effects of stiffness k, damping ratio ζ, and supported mass m on URN levels. For each model, two different masses are supported by the mounts. Table 1 details the testing parameters of four cases tested with different added masses. Natural frequencies f_n are computed according to Eq. (3). Static deflections d are measured with a caliper for each mount and compared to the manufacturer data. Experimental values correspond to the average deflection of the four mounts. The manufacturer's deflections were not available for Cases #2 and #4. Differences between deflections are 0.1 mm for both models, indicating the sufficient validity and accuracy of the physical properties provided by the manufacturer. Four mounts are installed at each corner between the plate supporting the shaker and the main structure of the platform, as shown in Fig. 11.

Table 1
Testing parameters for the four tested cases of elastic mounts with different added masses.

Testing parameter	Case #1	Case #2	Case #3	Case #4
Hardness [Shore]	40	40	70	70
Stiffness [kN/mm]	0.08	0.08	0.24	0.24
Damping ratio [–]	0.03	0.03	0.09	0.09
Mass [kg/mount]	20	30	80	20
Ratio of optimal mass [%]	100	150	100	25
Natural frequency [Hz]	10.1	8.2	8.7	17.4
Deflection (measured) [mm]	2.9	4.0	3.2	1.1
Deflection (manufacturer) [mm]	2.8	N/A	3.3	N/A

3.2. Mineral wool

Mineral wool used in marine constructions (bulkhead and deck) is selected as the sound-absorbing material (Rockwool SeaRox SL 620). Two coverage ratios are considered (40% and 70% coverage of the platform's interior surfaces, see Figs. 12 and 13). These two coverage ratios correspond to a 4 and 6% mass increase of the platform, respectively.

To get an order of magnitude of the attenuation brought by a very simplified system compared to the actual platform, simulations using the Transfer Matrix Method (TMM) were performed with the NOVA software (Mecanum inc., 2024). A mineral wool layer was simulated following the Johnson-Champoux-Allard (JCA) model (Allard and Atalla, 2009). Table 2 reports the mineral wool physical properties measured under laboratory conditions, including the values of the five macroscopic parameters required to model the material using the JCA model, namely the porosity, the tortuosity, the quasi-static airflow resistivity, and the two characteristic lengths. The mineral wool layer was considered homogeneous with a rigid frame and infinite lateral extent with some imperfections due to its positioning. These imperfections were considered by a 5% bare area over the panel using the parallel TMM approach, as proposed by Verdière et al. (2013). The mineral wool layer was coupled to an infinitely large flat steel panel, having the same thickness as the platform (6 mm). The excitation was supposed to be a diffuse acoustic field with a maximum incidence angle of 78° (field incidence). The sound transmission loss was first evaluated for a bare steel panel and then with an added layer of mineral wool. The theoretical insertion loss for this simplified system was calculated as the difference between the two calculated sound transmission loss values (in third-octave bands between 20 Hz and 2000 Hz).

3.3. Damping tiles

Damping tiles are used in the shipbuilding industry to reduce structure-borne noise by converting vibration energy to heat through viscous effects (Fischer, 2024). Damping tiles used in the marine sector (Pyrotek Decidamp) are selected. A 6 mm thickness is chosen to equal the platform's thickness and maximize effectiveness (Fischer, 2024).

Table 2
Measured physical properties of the mineral wool.

Physical property	Value
Thickness [mm]	50
Density [kg/m^3]	107.4
Open Porosity [–]	0.941
Resistivity [N s/m^4]	79 300
Tortuosity [–]	1
Viscous Length [μm]	16.2
Thermal Length [μm]	32.5

Table 3
Measured physical properties of the damping tiles.

Physical property	Value
Thickness [mm]	6
Dimensions [mm]	308 × 308
Young's modulus [MPa]	40 651
Loss factor [–]	0.1772

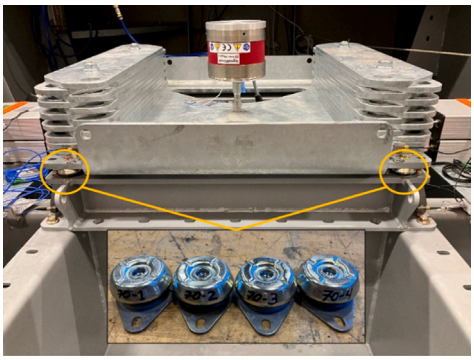

Fig. 11. Elastic mounts installation inside the platform.

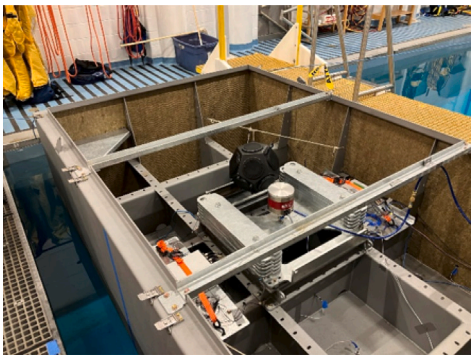

Fig. 12. Mineral wool installation inside the platform (40% surface coverage).

Table 3 presents the physical properties of the tiles measured under laboratory conditions. The tiles are mostly installed on the platform's bottom surface and vertically on the perimeter at the same height as the platform's draught (Fig. 14).

4. Results and discussion

4.1. Insertion loss evaluation

To evaluate insertion loss for a given technology, a linear average is done across the three hydrophones according to Eq. (5) to obtain underwater noise pressure levels L_p (referred by "URN" in Fig. 15 to 20 and Fig. 22 to 24) averaged over the water column for a given position

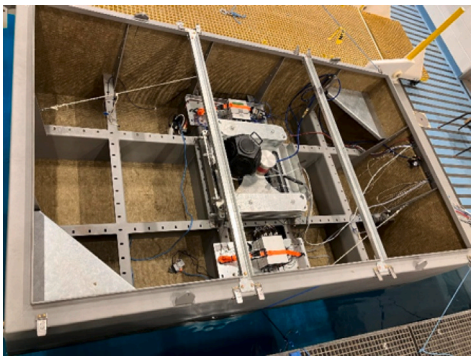

Fig. 13. Mineral wool installation inside the platform (70% surface coverage).

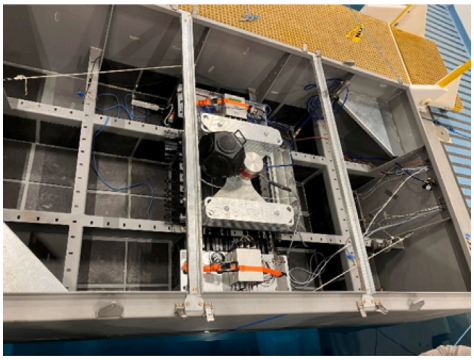

Fig. 14. Damping tiles installation inside the platform.

in the basin:

$$L_p = 10\log_{10}\left(\frac{1}{3}(10^{\frac{P_{1,dB}}{10}} + 10^{\frac{P_{2,dB}}{10}} + 10^{\frac{P_{3,dB}}{10}})\right), \quad (5)$$

where $P_{i,dB}$ corresponds to the dB level measured by hydrophone i.

A single hydrophone position within the basin is selected using the signal-to-noise ratio (SNR). Since these are closer to the platform, SNR is better for hydrophone positions 1 and 8 (Fig. 8). Fig. 15 compares the URN levels and SNR at those positions for the reference case without any mitigation technology installed on the platform. Both sources are fed up with pink noise. Third-octave bands are used to facilitate results analysis and interpretation.

SNR is larger at position P8 than at P1 up to the 400 Hz third-octave frequency band. Since machinery noise is mainly contained in that frequency domain, P8 (under the platform) is thus selected. To sum up, insertion loss (IL) corresponds to the difference in URN levels (averaged over three hydrophones) with and without mitigation technologies at position P8. Pink noise is used to evaluate insertion loss for the three mitigation technologies (Sections 4.3.1, 4.4 and 4.5).

4.2. Insertion loss uncertainty

Measurements at P8 with different technologies installed on the platform are not consecutive. There is an uncertainty associated with positioning the hydrophone array precisely at this position regarding the basin's modal behavior below 620 Hz, as discussed in Section 2.2. To quantify this uncertainty, three measurements with the same platform configuration are compared together. The hydrophone array was taken out of the basin and repositioned precisely between each measurement to evaluate the repeatability of the positioning system. Fig. 16 compares the three measurements for the shaker and the speaker, functioning separately and fed by pink noise, to isolate the structure-borne and airborne noise uncertainty.

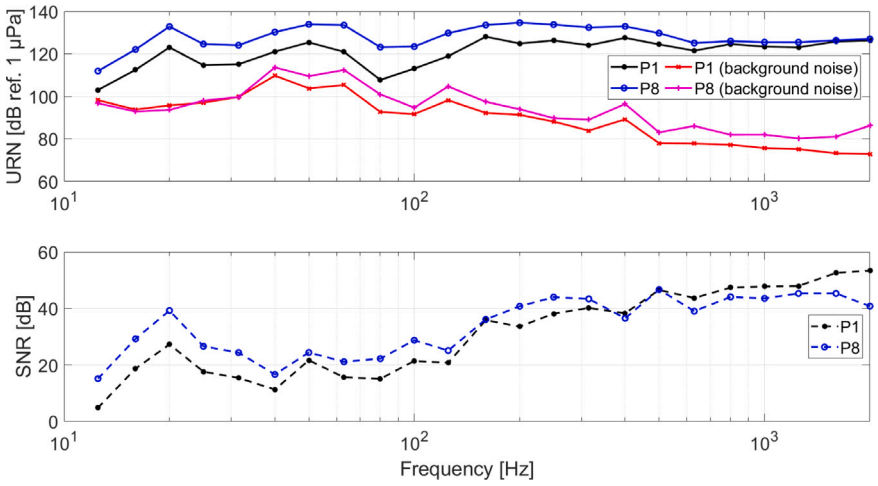

Fig. 15. (Top figure) Measured URN and background noise at P1 and P8. – (Bottom figure) Corresponding signal-to-noise ratio (SNR).

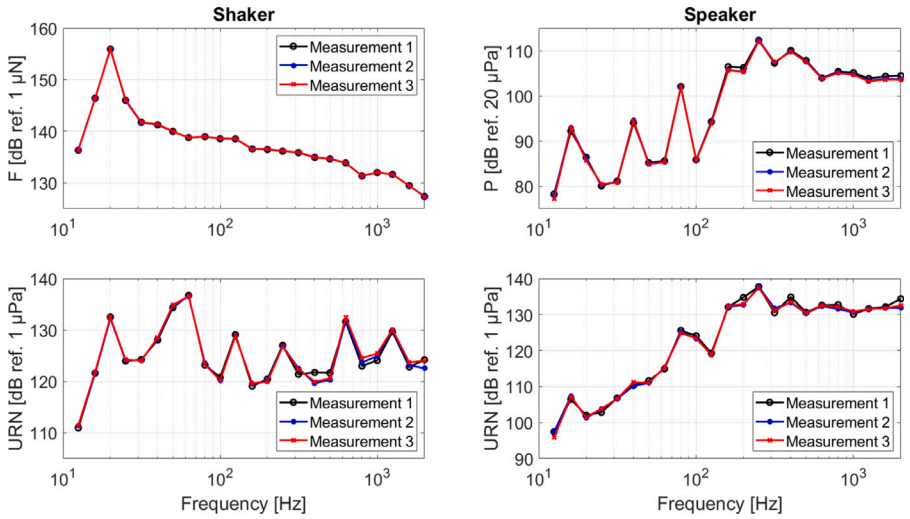

Fig. 16. Comparison in URN levels for three different measurements at P8. (Left) Injected force and corresponding URN for the shaker. – (Right) Injected noise and corresponding URN for the speaker.

Injected force and injected noise are similar for the three measurements: differences in URN levels are due to hydrophone positioning. Maximum differences between two measurements of 2 dB and 3 dB are observed for the shaker and speaker, respectively. Averaging the maximum differences across all third-octave bands, a 1 dB average difference is obtained for the two sources, showing that the developed methodology provides repeatable measurements. As expected, URN variability increases with frequency: URN levels in the basin become more sensitive to slight differences in hydrophone positions as frequency increases because of smaller wavelengths. The maximum differences between two measurements for a given third-octave band correspond to the insertion loss uncertainty associated with hydrophone positioning, presented as vertical lines in Figs. 17, 18, 22 and 24.

4.3. Elastic mounts

4.3.1. Insertion loss

The shaker is used separately to isolate the mounts' effect on structure-borne noise. Figs. 17 and 18 present URN and insertion loss for Case #1 and #3 (see Table 1), respectively. URN levels are presented in narrow bands (1 Hz resolution), while insertion losses are averaged over third-octave bands to illustrate broadband effects. Background noise is also presented.

Both models provide significant URN reductions from the 31.5 Hz third-octave band. Up to 37 dB reductions are obtained at 200 Hz (Case #1). Some reductions could not be fully observed for some frequencies as URN levels drop to the background noise floor (see 70 to 200 Hz, for example, Fig. 17). For those frequencies, the insertion loss might then be underestimated. Generally, lower stiffness mounts (Case #1) provide higher insertion loss over the whole frequency spectrum. Results show that, in this case, stiffer mounts do not lead to improved insertion loss. Also, URN levels are amplified around 12 Hz and 17 Hz for Cases #1 and #3, respectively. The mounts' mechanical resonances cause this amplification: to avoid amplifying structure-borne noise near resonance, it is thus essential to properly design elastic mounts such that the natural frequency is far from the lowest operating frequency of the machine to be isolated.

4.3.2. Effect of loading

The effect of mounts' loading on URN is also investigated. Fig. 19 presents measured URN for Case #1 and #2, while Case #3 and #4 are presented in Fig. 20. Each loading case with mounts is compared to a bare platform with the same loading to ensure a similar wetted surface, except for Case #2. The data were unavailable for the reference bare Case #2 without mounts: the comparison is made instead with Case #1 load.

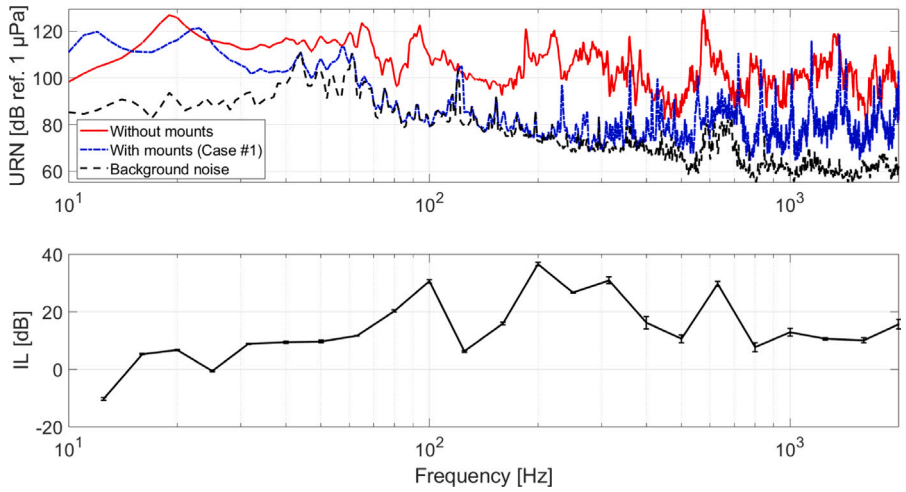

Fig. 17. Case #1 (see Table 1) – (Top) Measured URN with and without elastic mounts. – (Bottom) Corresponding insertion loss. Vertical lines correspond to the structure-borne uncertainty, as evaluated in Section 4.2.

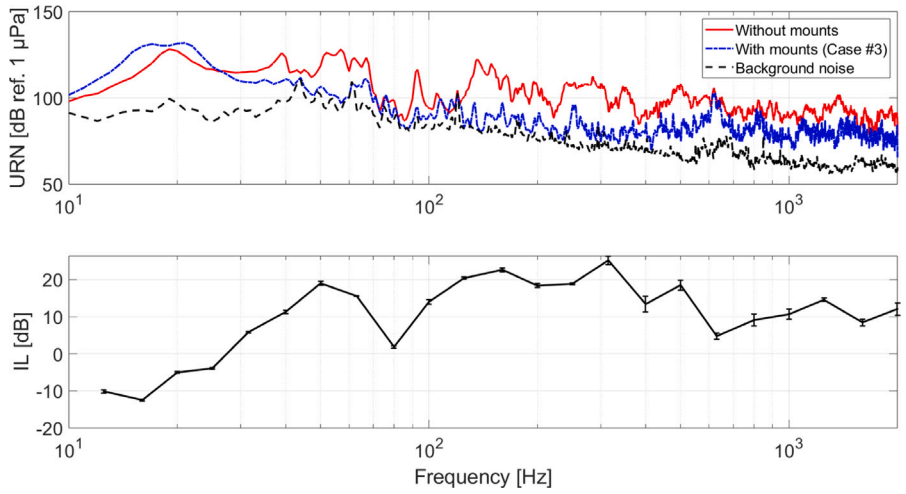

Fig. 18. Case #3 (see Table 1) – (Top) Measured URN with and without elastic mounts. – (Bottom) Corresponding insertion loss. Vertical lines correspond to the structure-borne uncertainty, as evaluated in Section 4.2.

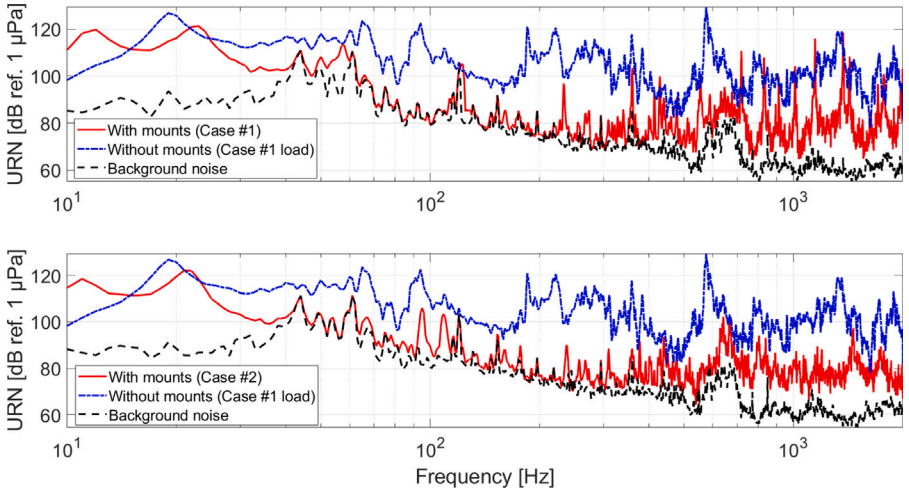

Fig. 19. URN with and without mounts – (Top) Case #1. – (Bottom) Case #2.

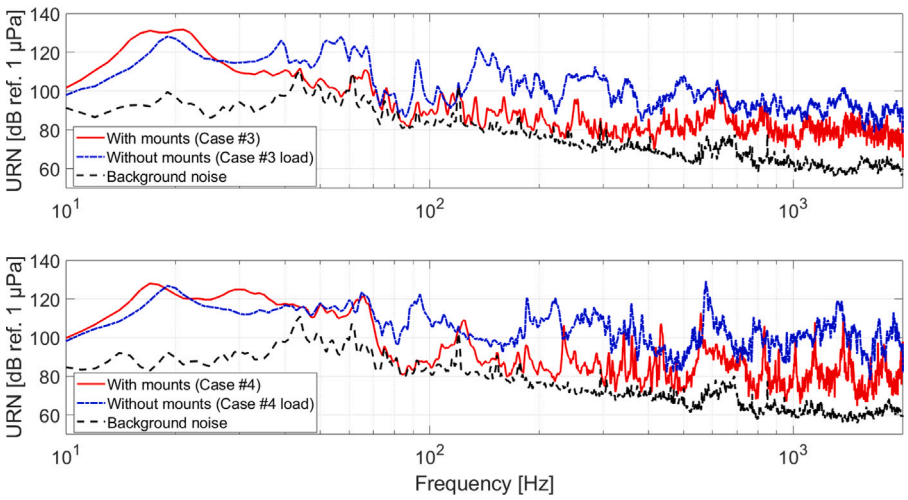

Fig. 20. URN with and without mounts – (Top) Case #3. – (Bottom) Case #4.

The mounts' resonance is slightly shifted towards lower frequencies for Case #2 (mounts loaded at 150% of their capacity). This is expected since resonance frequency f_n is inversely proportional to mass according to Eq. (3). Except for the shift in resonance frequency, no significant differences are observed between Case #1 and #2: both provide significant URN reductions from 25 Hz. However, exceeding the mechanical loading on mounts is generally not recommended as it will decrease their lifespan. Regarding Case #4 (mounts loaded at 25%), resonance is shifted towards higher frequencies since mass decreases, thus increasing the risk of overlapping with a machine's operating frequencies. Significant URN reductions are observed starting from 25 Hz for Case #3 (100% loading), whereas it only begins above 70 Hz for Case #4 (25% loading). Improved vibration isolation is thus achieved with optimal loading (100%). Results highlight the importance of respecting the mounts' optimal load capacity to maximize their lifespan and vibration isolation. To meet this requirement, the total mass of the machine to be isolated, including all accessories (pipes, protections, etc.), must be known to select and properly design the mounts. Along with the supported mass m, the preload or initial compression applied to the mount, not considered in this study, is also an important parameter: its increase leads to a higher dynamic stiffness k, shifting the natural frequency of the system f_n towards higher frequencies (Fragasso and Moro, 2022).

4.3.3. Transmissibility

Along with URN levels, acceleration levels inside the platform are also analyzed to evaluate the transmissibility of both models of mounts. The ratio of the linear average acceleration levels before (A_{in}) and after (A_{out}) the mount is computed to obtain the experimental transmissibility T_{exp} according to Eq. (6) (Fragasso and Moro, 2022):

$$T_{exp} = \frac{A_{out}}{A_{in}} = \frac{\sum_{n=1}^{4} 10^{\frac{A_{n,out}}{10}}}{\sum_{n=1}^{4} 10^{\frac{A_{n,in}}{10}}}, \tag{6}$$

where n is the mount number and $A_{n,in}$ and $A_{n,out}$ are the acceleration levels (in dB) for a given mount n on the top and bottom surface of the mount, respectively. Fig. 21 presents the experimental transmissibility for Case #1 and #3, both with optimal loading (100%). Using the mounts' physical parameters from Table 1 and Eq. (4), theoretical transmissibilities are also presented.

Experimental transmissibilities are close to unity when $f/f_n < 1$ and start to decrease around natural frequencies, but not exactly at $f/f_n = 1$. This could be due to the fact that physical parameters (Table 1) used to calculate natural frequency with Eq. (3) are not completely accurate. It is shown that transmissibility is lower over most of the frequency spectrum above natural frequency for Case #1: in this case, softer mounts (lower damping ratio ζ) lead to better isolation. This is coherent with the URN data since the highest insertion losses are obtained with Case #1 (see Figs. 17 and 18). This tendency also corresponds to the theoretical curves: a smaller damping ratio ζ leads to lower transmissibility in the $f \geq \sqrt{2} f_n$ region as shown in Fig. 10. The order of magnitude of experimental versus theoretical transmissibilities is similar, indicating that Eq. (4) can be used as a first approximation to estimate vibration isolation. However, results clearly show that non-negligible disparities are observed between experiment and theory. Analytical models can thus represent general tendencies, but experiments or accurate numerical modeling should be conducted through the design phase as proposed in Fragasso and Moro (2022) and Fragasso et al. (2019) to capture adequately complex structural behaviors.

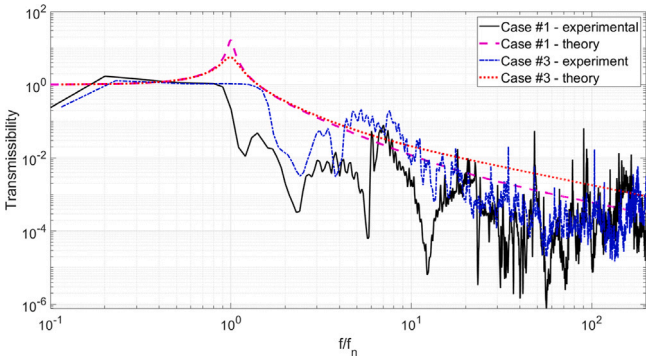

Fig. 21. Comparison between experimental and theoretical transmissibility for Cases #1 and #3 (100% loading).

4.4. Mineral wool

Since mineral wool targets airborne noise, insertion loss is evaluated only with the speaker functioning. Fig. 22 shows the URN and the insertion loss for the two configurations. Results from the simplified numerical simulation (JCA model described in Section 3.2) are also shown.

Implementing mineral wool can reduce significantly (up to 20 dB) the airborne contribution to URN over 160 Hz, which is consistent with the material's technical absorption curve. Reductions up to 20 dB are obtained with 70% surface coverage. This reduction in magnitude

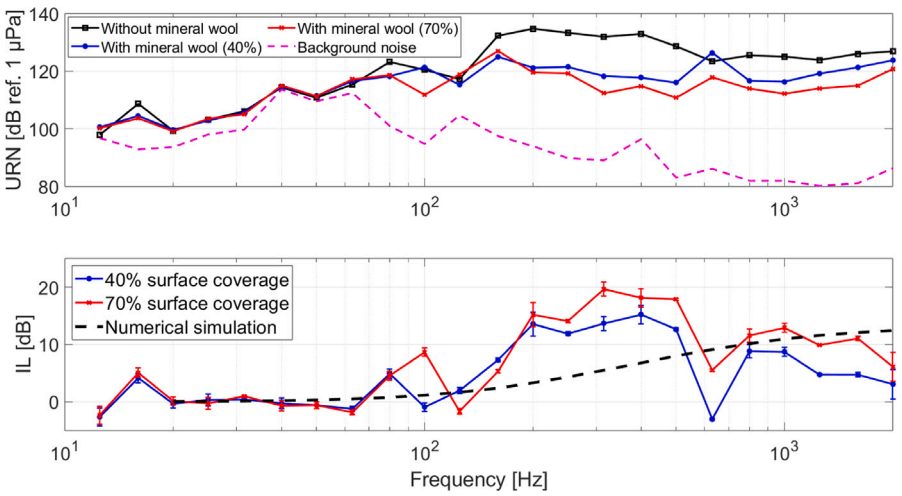

Fig. 22. (Top figure) Measured URN with and without mineral wool for the two surface coverages. – (Bottom figure) Corresponding insertion loss. Vertical lines correspond to the airborne uncertainty.

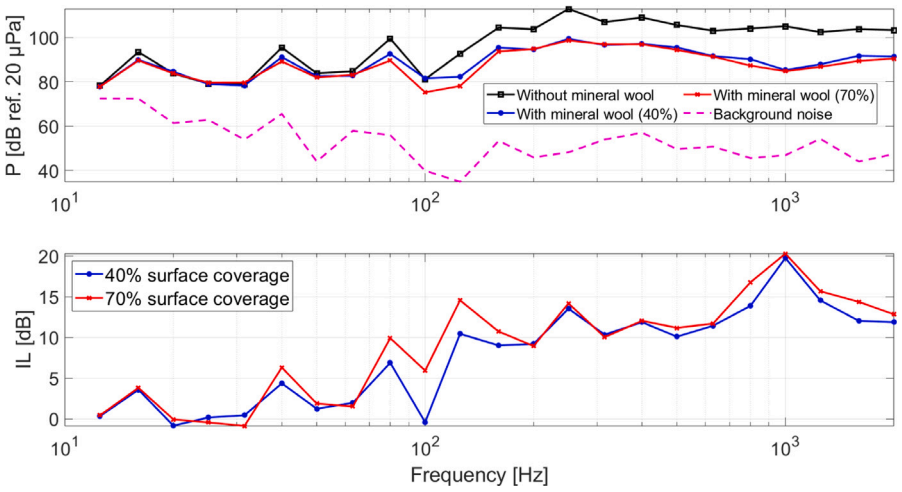

Fig. 23. (Top) Measured noise inside the platform with and without mineral wool for the two surface coverage. – (Bottom) Corresponding insertion loss.

is consistent with results obtained by Dylejko et al. (2016) from an analytical model that predicts the effect of this type of material. The lack of reduction in low frequency can be explained by the thickness of the used mineral wool. Indeed, the rule of thumb for a passive sound-absorbing material to be fully effective is to have a thickness at least equal to a quarter of the wavelength to be attenuated ($\lambda/4$). For example, at 63 Hz, the wavelength in the air ($c = 343$ m/s) is around 5 m, so the mineral wool should have a thickness of around 1.25 m, which is highly impractical in an engine room. With a thickness of 50 mm, mineral wool is, therefore, ineffective at low frequencies. Also, increasing the amount of covered surface from 40% to 70% offers significant gains in insertion loss from 200 Hz. Indeed, gains up to 9 dB (630 Hz third-octave band) are obtained with the 70% configuration. It indicates that the larger the surface coverage ratio, the better the effectiveness in reducing the airborne contribution to underwater radiated noise.

Regarding the numerical simulation, the infinite plate model insertion loss (IL) matches the experimental one up to 125 Hz and from the 630 Hz third-octave bands, particularly for the 70% surface coverage. The simulation insertion loss underestimates experimental data in between those bands. Results show that a simplified numerical model can capture general tendencies compared to actual testing. This indicates that a more complex numerical model could be used to predict accurately and optimize the effectiveness given by a particular technology with known physical parameters.

Along with URN, corresponding noise levels inside the platform are also analyzed to investigate the absorption effects of mineral wool. Fig. 23 presents noise inside the platform and insertion loss for the two configurations. Noise levels correspond to the linear average of the two microphones inside the platform.

Significant noise reductions (up to 20 dB) are obtained from the 125 Hz third-octave band, consistent with the URN reductions. Considering that workers in engine rooms are subject to high levels of hazardous noise throughout their daily shifts, installing sound-absorbing materials in an engine room could be doubly beneficial: it simultaneously reduces URN and airborne noise, improving both the marine and crews' environments.

4.5. Damping tiles

The shaker alone is used to isolate the effect of damping tiles on the structure-borne contribution to URN. Fig. 24 presents URN and corresponding insertion loss.

No significant broadband effect of damping tiles on URN is observed. Some differences between the reference case and the one with the tiles are observed above 200 Hz, but no general trend is present: URN levels with tiles are sometimes higher, sometimes lower than without tiles. Operating temperature, installation method and type could explain the absence of reduction effects. Indeed, the selected damping

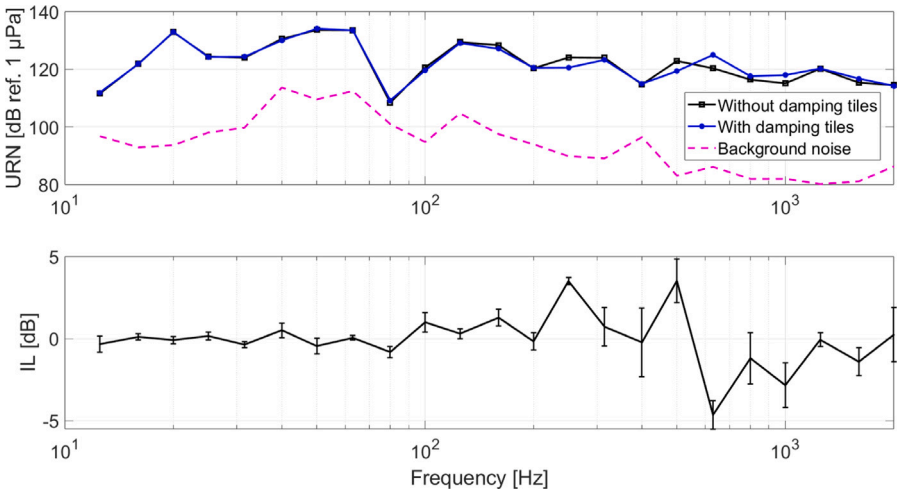

Fig. 24. (Top figure) Measured URN with and without damping tiles. – (Bottom figure) Corresponding insertion loss. Vertical lines correspond to the structure-borne uncertainty.

Table 4
Average insertion loss for the tested technologies.

Technology	Insertion loss [dB]			
	Low $12.5 \leq f \leq 100$ Hz	Mid $100 < f \leq 1000$ Hz	High $1000 < f \leq 2000$ Hz	Overall $12.5 \leq f \leq 2000$ Hz
Elastic mounts – Case #1	9	19	12	14
Elastic mounts – Case #3	4	16	12	10
Mineral wool – 40% coverage	0	9	4	5
Mineral wool – 70% coverage	1	12	9	7
Damping tiles	0	0	0	0

tiles are designed to offer maximal damping performance around 60 °C. The operating temperature on the platform was around 20 °C, which is therefore not optimal. Insertion loss might increase in an actual engine room where the operating temperature is generally higher than 20 °C. Additionally, the tiles were fixed with a removable silicone sealant to re-use the platform for future testing. Hence, the installation method could also be responsible for the absence of a broadband reduction effect on the URN of the damping tiles. Finally, the damping tiles were installed as an unconstrained layer, which reduces structural resonance more effectively than offers a broadband effect. This type of installation is not as effective as a constrained layer in which the tiles are fixed to the base structure, and a covering plate is installed on top since induced shearing effects are more important (Fischer, 2024). An improved installation method and operating temperature could allow to state if the lack of URN reduction is actually due to the tiles themselves.

4.6. Synthesis

Table 4 presents the average insertion loss for the different technologies for low, mid, and high frequencies. An overall average is also presented. Overall, elastic mounts are better at reducing structure-borne noise than mineral wool is at reducing airborne noise for the whole frequency spectrum. Better reductions are obtained for mid and high frequency for both technologies. Mounts can reduce structure-borne noise at low frequency, whereas mineral wool does not attenuate airborne noise. Damping tiles do not provide wide-band reductions. Suppose only one technology must be selected to reduce the contribution from a machine: in that case, results show that elastic mounts should be prioritized over mineral wool and damping tiles, considering structure-borne noise is generally dominant over airborne noise. However, the airborne noise contribution to URN would be unaffected. Therefore, a complementary solution consisting of a combination of both is ideal to target both transmission paths simultaneously.

5. Conclusions and perspectives

As highlighted by the recent 2023 IMO guidelines, there is a need to find practical solutions for reducing underwater radiated noise from commercial shipping, which has adverse impacts on marine life. Targeting specifically machinery noise through standard mitigation technologies reduces ships' underwater radiated noise as it is the primary noise source at low speeds. The actual incorporation of such technologies of ships is, however, lacking. At the same time, concrete gains associated with each are currently unknown due to the cost and complexity of conducting on-ship testing. Testing at a smaller scale offers a faster and low-cost solution and provides a controlled environment, which is challenging to obtain on an actual ship. Several studies followed this path using testing structures in water basins, but none focused on URN reductions given by standard mitigation technologies.

In this study, a test structure representative of a ship section is designed and deployed in a water basin. It is shown that repeatable and accurate insertion loss evaluation can be made in a reverberant basin if its acoustic response is first characterized, and a precise hydrophone positioning system is used. Up to 37 dB and 20 dB URN reductions are obtained with elastic mounts and mineral wool, respectively. Regarding damping tiles, future testing must state if the installation method and operating temperature are responsible for the lack of reduction. The observed URN reductions are limited by the background noise for some frequency bands. Insertion loss might then be underestimated for those bands. To avoid this limitation, more powerful sources could be used or machines surrounding the basin could be turned off in future works to increase the signal-to-noise ratio.

The developed platform and repeatable methodology presented in this study fill a technological gap by quantifying the actual URN reductions given by noise control technologies currently used on ships (elastic mounts, mineral wool and damping tiles). The study's main limitation is that the vibroacoustic phenomena of a real vessel are not reproduced by the platform since a reference ship with a scaling law was not used. The platform's acoustic and structural modal

behaviors then differ from a real vessel's (low-frequency vibration modes corresponding to global modes, possibly additional vibroacoustic transmission paths). However, quantifying the URN reductions at a small scale in a controlled environment constitutes a first step to clarify the cost-effectiveness ratio (dB/$) of URN reduction measures, as highlighted by the 2023 IMO guidelines. Clarifying the dB part of this ratio reduces shipowners' monetary risk and can give incentives to incorporate mitigation technologies while designing or retrofitting a ship. The platform also allows for a better understanding of the parameters involved in designing ship noise control technologies, providing better guidelines for naval architects and engineers.

In future works, the platform and developed methodology could be used to test and quantify the effectiveness of other mitigation technologies used on ships, thus continuing to bridge the technological gap regarding the lack of quantitative data on URN reduction technologies. It could also be used to conduct transfer path analysis independently using the two sources from both the mechanical and acoustic standpoints. Parameters such as radiation efficiency and acoustic directivity could be obtained to better understand the relative contributions to URN of structure-borne and airborne noise. This would allow to identify the dominant transmission path to target while selecting mitigation technologies on ships. Finally, this study assessed the effectiveness of several mitigation technologies from an experimental point of view. Results show that a simplified numerical model can capture general tendencies observed experimentally. Therefore, the acquired experimental data are used in ongoing work to develop and validate the accuracy of a more complex finite-element model of the whole platform. The model will allow to predict URN levels and model noise radiation in the basin. Given the controlled environment, the validity of experimental versus numerical results could also be assessed. Such a numerical model could then be used to optimize the effectiveness of mitigation solutions before basin trials and their adoption on real ships. Modal analysis could also be conducted to study the structural properties of the platform and facilitate the interpretation of results.

Overall, the platform and the developed methodology can support and guide the implementation of mitigation measures in current and future ship constructions. Shipyards, shipowners, and naval engineers can benefit directly from the expertise and knowledge developed.

CRediT authorship contribution statement

Marc-André Guy: Writing – review & editing, Writing – original draft, Visualization, Validation, Software, Methodology, Investigation, Formal analysis, Data curation. **Kamal Kesour:** Writing – review & editing, Validation, Supervision, Resources, Project administration, Methodology, Funding acquisition, Conceptualization. **Mathis Vulliez:** Investigation. **Stéphane Gagnon:** Resources, Investigation. **Julien St-Jacques:** Resources, Investigation. **Raphael Tremblay:** Resources. **Jean-Christophe Gauthier Marquis:** Resources, Funding acquisition. **Olivier Robin:** Writing – review & editing, Visualization, Validation, Supervision, Resources, Project administration, Methodology, Funding acquisition, Conceptualization.

Declaration of competing interest

The authors declare that they have no known competing financial interests or personal relationships that could have appeared to influence the work reported in this paper.

Data availability

Data will be made available on request.

Acknowledgments

This work was supported by Transport Canada through the Quiet Vessel Initiative (Grant no. 164627); Davie Shipyard; and Mitacs (Accelerate Program, Grant no. IT38066). The authors thank André Cyr, Jean-David Godin, Simon St-Pierre, Gabriel Dugas and Bira Dos Reis Brunet for the CAD design and stability study of the platform and Mecanum Inc. for providing equipment for mineral wool and damping tiles testing.

References

Abrahamsen, K., 2012. The ship as an underwater noise source. In: Proceedings of Meetings on Acoustics. 070058. http://dx.doi.org/10.1121/1.4772953.

Allard, J., Atalla, N., 2009. Propagation of Sound in Porous Media: Modelling Sound Absorbing Materials. John Wiley & Sons.

Andrew, R., Howe, B., Mercer, J., 2010. Long-time trends in low-frequency traffic noise for four sites off the north american west coast. J. Acoust. Soc. Am. 127 (1783), http://dx.doi.org/10.1121/1.3383944.

Andrew, R.K., Howe, B.M., Mercer, J.A., Dzieciuch, M.A., 2002. Ocean ambient sound: Comparing the 1960s with the 1990s for a receiver off the california coast. Acoust. Res. Lett. Online 3, 65–70. http://dx.doi.org/10.1121/1.1461915.

Armelloni, E., Falkner, R., Rako Gospić, N., Radulovic, M., Pleslić, G., Muslim, S., Mihanović, H., Gaggero, T., 2022. Characterization of the underwater noise produced by recreational and small fishing boats (< 14 m) in the shallow-water of the cres-lošinj natura 2000 sci. Mar. Pollut. Bull. 183, 114050. http://dx.doi.org/10.1016/j.marpolbul.2022.114050.

Arveson, P., Vendittis, D., 2000. Radiated noise characteristics of a modern cargo ship. J. Acoust. Soc. Am. 107, 118–129. http://dx.doi.org/10.1121/1.428344.

Audoly, C., Gaggero, T., Baudin, E., Folegot, T., Rizzuto, E., Mullor, R., André, M., Rousset, C., Kellett, P., 2017. Mitigation of underwater radiated noise related to shipping and its impact on marine life: A practical approach developed in the scope of aquo project. IEEE J. Ocean. Eng. PP, 1–16. http://dx.doi.org/10.1109/JOE.2017.2673938.

Audoly, C., Rousset, C., Salinas-Mullor, R., Rizzuto, E., Hallander, J., Baudin, E., 2015. Mitigation measures for controlling the ship underwater radiated noise, in the scope of aquo project. In: IEEE. http://dx.doi.org/10.1109/OCEANS-Genova.2015.7271381.

Cochard, N., Lacoume, J.L., Arzelies, P., Gabillet, Y., 2000. Underwater acoustic noise measurement in test tanks. IEEE J. Ocean. Eng. 25, 516–522. http://dx.doi.org/10.1109/48.895359.

Çorakçı, A.C., Biber, A., Saydam, T., Aksoy, S., 2024. Application of 2e-2u method for free-field underwater calibrations of hydrophones and projectors in a reverberant laboratory test tank. Meas. Sci. Technol. 35, 085002. http://dx.doi.org/10.1088/1361-6501/ad42be.

Donaldson, J., 1968. Reduction of noise radiated from ship structures. Appl. Acoust. 1, 275–291. http://dx.doi.org/10.1016/0003-682X(68)90029-7.

Dylejko, P., MacGillivray, I., Moore, S., Skvortsov, A., 2016. The influence of internal resonances from machinery mounts on radiated noise from ships. IEEE J. Ocean. Eng. PP, 1–11. http://dx.doi.org/10.1109/JOE.2016.2593648.

Erbe, C., Marley, S., Schoeman, R., Smith, J., Trigg, L., Embling, C., 2019. The effects of ship noise on marine mammals—a review. Front. Mar. Sci. 6, http://dx.doi.org/10.3389/fmars.2019.00606.

Fischer, R., 2024. Noise and Vibration Control on Ships - Understanding and Cutting Through the Noise. John Wiley & Sons.

Fragasso, J., Helal, K., Moro, L., 2024. Transfer-path analysis to estimate underwater radiated noise from onboard structure-borne sources. Appl. Ocean Res. 147, 103979. http://dx.doi.org/10.1016/j.apor.2024.103979.

Fragasso, J., Moro, L., 2022. Structure-borne noise of marine diesel engines: Dynamic characterization of resilient mounts. Ocean Eng. 261, 112116. http://dx.doi.org/10.1016/j.oceaneng.2022.112116.

Fragasso, J., Moro, L., Lye, L.M., Quinton, B.W., 2019. Characterization of resilient mounts for marine diesel engines: Prediction of static response via nonlinear analysis and response surface methodology. Ocean Eng. 171, 14–24. http://dx.doi.org/10.1016/j.oceaneng.2018.10.051.

Frisk, G., 2012. Noiseonomics: The relationship between ambient noise levels in the sea and global economic trends. Sci. Rep. 2 (437), http://dx.doi.org/10.1038/srep00437.

Gervaise, C., Simard, Y., Roy, N., Kinda, G., Ménard, N., 2012. Shipping noise in whale habitat: Characteristics, sources, budget, and impact on belugas in saguenay-st. lawrence marine park hub. J. Acoust. Soc. Am. 132, 76–89. http://dx.doi.org/10.1121/1.4728190.

Gigot, M., Tremblay, R., Bonnel, J., Mathias, D., Meziane, T., Chauvaud, L., Olivier, F., 2024. Noise pollution causes parental stress on marine invertebrates, the giant scallop example. Mar. Pollut. Bull. 203, 116454. http://dx.doi.org/10.1016/j.marpolbul.2024.116454.

Hildebrand, J., 2009. Anthropogenic and natural sources of ambient noise in the ocean. Mar. Ecol. - Prog. Ser. 395, 5–20. http://dx.doi.org/10.3354/meps08353.

International Maritime Organization, 2023. Revised Guidelines for the Reduction of Underwater Radiated Noise from Shipping To Address Adverse Impacts on Marine Life. Technical Report, International Maritime Organization (IMO).

International Organization for Standardization, 2008. ISO 3382-2:2008 Acoustics — Measurement of Room Acoustic Parameters Part 2: Reverberation Time in Ordinary Rooms. Technical Report, International Organization for Standardization (ISO).

István, L.V., Beranek, L.L., 2005. Noise and Vibration Control Engineering: Principles and Applications. John Wiley & Sons, http://dx.doi.org/10.1002/9780470172568.

ITTC, 2017. Underwater Noise from Ships, Full Scale Measurements. Technical Report, International Towing basin Conference (ITTC).

Kaplan, M., Solomon, S., 2016. A coming boom in commercial shipping? the potential for rapid growth of noise from commercial ships by 2030. Mar. Policy 73, 119–121. http://dx.doi.org/10.1016/j.marpol.2016.07.024.

Keizer, T., Gaudel, R., Goedbloed, I., 2022. Accuracy of numerically predicted underwater sound of a ship-like structure. In: Proceedings of Meetings on Acoustics. http://dx.doi.org/10.1121/2.0001565.

Kendrick, A., Terweij, R., 2019. Ship Underwater Radiated Noise. Technical Report, Vard Marine Inc.

Kuttruff, H., 2016. Room Acoustics. Crc Press.

Lee, J.Y., Cho, D.S., Kim, K., Park, S.J., 2024. Experimental validation on structure-borne underwater radiated noise transfer function analysis for marine structure. Int. J. Nav. Archit. Ocean Eng. 16, 100585. http://dx.doi.org/10.1016/j.ijnaoe.2024.100585.

Lee, J.Y., Kim, K., Park, S.J., Cho, D.S., 2023. Applicability and reliability of an experimental method measuring underwater acoustic radiation efficiency of floating box-type plate structures in a reverberant water tank. Int. J. Nav. Archit. Ocean Eng. 15, 100553. http://dx.doi.org/10.1016/j.ijnaoe.2023.100553.

Lloyd, T., Lafeber, F.H., Bosschers, J., 2024. Ship urn mitigation by air injection: model-scale experiments and application to full-scale measurement data. In: 8th International Symposium on Marine Propulsors (SMP 2024). http://dx.doi.org/10.15480/882.9336.

Lloyd, T., Lafeber, F.H., Bosschers, J., Kaydihan, L., Boerrigter, B., 2023. Scale model measurements of ship machinery noise mitigation by air injection. In: 7th International Conference on Advanced Model Measurement Technology for the Maritime Industry (AMT'23).

Mcdonald, M., Hildebrand, J., Wiggins, S., Ross, D., 2008. A 50 year comparison of ambient ocean noise near san clemente island: A bathymetrically complex coastal region off southern california. J. Acoust. Soc. Am. 124, 1985–1992. http://dx.doi.org/10.1121/1.2967889.

McKenna, M., Ross, D., Wiggins, S., Hildebrand, J., 2012. Underwater radiated noise from modern commercial ships. J. Acoust. Soc. Am. 131, 92–103. http://dx.doi.org/10.1121/1.3664100.

Mecanum inc., 2024. Nova - simulator of multilayer acoustic materials. URL https://mecanum.com/software/nova/.

Murchy, K., Davies, H., Shafer, H., Cox, K., Nikolich, K., Juanes, F., 2019. Impacts of noise on the behavior and physiology of marine invertebrates: A meta-analysis. In: Proceedings of Meetings on Acoustics. 040002. http://dx.doi.org/10.1121/2.0001217.

Possenti, L., De Nooijer, L., de Jong, C., Lam, F.P., Beelen, S., Bosschers, J., Terwisga, T., Stigter, R., Reichart, G.J., 2024. The present and future contribution of ships to the underwater soundscape. Front. Mar. Sci. 11, http://dx.doi.org/10.3389/fmars.2024.1252901.

Possenti, L., reichart, g.j., De Nooijer, L., lam, f.p., de Jong, C., colin, m., binnerts, b., heydt, a., 2023. Predicting the contribution of climate change on north atlantic underwater sound propagation. PeerJ http://dx.doi.org/10.7717/peerj.16208.

Putland, R., Merchant, N., Farcas, A., Radford, C., 2017. Vessel noise cuts down communication space for vocalising fish and marine mammals. Glob. Change Biol. 24, http://dx.doi.org/10.1111/gcb.13996.

Robinson, S., Harris, P., Cheong, S.H., Wang, L., Livina, V., Haralabus, G., Zampolli, M., Nielsen, P., 2023. Impact of the covid-19 pandemic on levels of deep-ocean acoustic noise. Sci. Rep. 13, http://dx.doi.org/10.1038/s41598-023-31376-3.

Ryan, J., Joseph, J., Margolina, T., Hatch, L., Azzara, A., Reyes, A., Southall, B., DeVogelaere, A., Peavey Reeves, L., Zhang, Y., Cline, D., Jones, B., McGill, P., Baumann-Pickering, S., Stimpert, A., 2021. Reduction of low-frequency vessel noise in monterey bay national marine sanctuary during the covid-19 pandemic. Front. Mar. Sci. 8, http://dx.doi.org/10.3389/fmars.2021.656566.

Schroeder, M., 1965. New method of measuring reverberation time. J. Acoust. Soc. Am. 37, 409–412. http://dx.doi.org/10.1121/1.1909343.

Schroeder, M.R., 1996. The Schroeder frequency revisited. J. Acoust. Soc. Am. 99, 3240–3241. http://dx.doi.org/10.1121/1.414868.

Smith, T.A., Grech La Rosa, A., Wood, B., 2024. Underwater radiated noise from small craft in shallow water: Effects of speed and running attitude. Ocean Eng. 306, 118040. http://dx.doi.org/10.1016/j.oceaneng.2024.118040.

Smith, T., Rigby, J., 2022. Underwater radiated noise from marine vessels: A review of noise reduction methods and technology. Ocean Eng. 266, 112863. http://dx.doi.org/10.1016/j.oceaneng.2022.112863.

Terry, C., Rothendler, M., Zipf, L., Dietze, M.C., Primack, R.B., 2021. Effects of the covid-19 pandemic on noise pollution in three protected areas in metropolitan boston (usa). Biol. Conserv. 256, 109039.

Tournadre, J., 2014. Anthropogenic pressure on the open ocean: The growth of ship traffic revealed by altimeter data analysis. Geophys. Res. Lett. 41, 7924–7932. http://dx.doi.org/10.1002/2014GL061786.

Trinh, V., Chen, L., Forrest, J., 2018. Free-field acoustic source levels from measurements conducted in a water basin. In: Hear to Listen - Acoustics Adelaide South Australia.

Verdière, K., Panneton, R., Elkoun, S., Dupont, T., Leclaire, P., 2013. Transfer matrix method applied to the parallel assembly of sound absorbing materials. J. Acoust. Soc. Am. 134, 4648–4658. http://dx.doi.org/10.1121/1.4824839.

Williams, R., Wright, A., Ashe, E., Blight, L., Bruintjes, R., Canessa, R., Clark, C., Cullis-Suzuki, S., Dakin, T., Erbe, C., Hammond, P., Merchant, N., hara, O., Purser, J., Radford, A., Simpson, S., Thomas, L., Wale, M., O'Hara, P., 2015. Impacts of anthropogenic noise on marine life: Publication patterns, new discoveries, and future directions in research and management. Ocean Coast. Manag. 115, 17–24. http://dx.doi.org/10.1016/j.ocecoaman.2015.05.021.

Zambon, G., Confalonieri, C., Angelini, F., Benocci, R., 2021. Effects of covid-19 outbreak on the sound environment of the city of milan, italy. Noise Mapp. 8, 116–128.

Zhang, Y.M., Tang, R., Li, Q., Shang, D.J., 2018. The low-frequency sound power measuring technique for an underwater source in a non-anechoic tank. Meas. Sci. Technol. 29, 035101. http://dx.doi.org/10.1088/1361-6501/aa9f6e.